Journal of Non-Crystalline Solids 604 (2023) 122130

Contents lists available at ScienceDirect

Journal of Non-Crystalline Solids

journal homepage: www.elsevier.com/locate/jnoncrysol

Boron-rich amorphous boron oxides from ab initio simulations

Ayşegül Özlem Çetin Karacaoğlan, Murat Durandurdu *

Nanotechnology Engineering & Materials Science and Mechanical Engineering Program, Abdullah Gül University, Kayseri, Turkey

ARTICLE INFO

Keywords:
Boron-rich
Boron oxides
Amorphous
ab initio

ABSTRACT

Amorphous boron oxide (B_xO_{1-x}, $0.5 \leq x \leq 95$) configurations are simulated by means of an *ab initio* molecular dynamics technique and their microstructure and mechanical properties are revealed in details. With increasing B content, the average B-coordination noticeably increases from 3.18 to 5.62 whereas the O-coordination, surprisingly, remains almost null, about 2.0. The formation of complete B_{12} molecules is observed after 80% B concentrations. Chemical segregation is witnessed in most models and hence the resulting configurations show B: B_2O_3 phase separations. The mechanical properties (bulk, shear and Young moduli, Vickers hardness and microhardness) substantially increase with increasing B content. The amorphous materials (B_xO_{1-x}, $x \geq 80$) are classified as hard materials. Within the limitations of DFT calculations and approaches used, we speculate that there is a ductile-to-brittle transition at around 70–75% B contents.

1. Introduction

The development of novel materials plays an important continuing role in the progression of the advanced technology. These novel materials can be classified as the corrosion-, erosion-, oxidation- and wear-resistant material systems [1]. Especially the wear-resistant materials/composites have drawn remarkable attentions due to both the increasing production demands in efficiency and the stimulations of new potential application areas [2]. The wear-resistant systems are generally qualified by high fracture toughness and high hardness. For this reason, these systems must be in the class of extremely-hard materials or super-hard materials [2]. Two well-known hardest materials are diamond and cubic boron nitride (c-BN). Diamond can be used in many applications requiring the extreme wear resistance. c-BN can be also used in many areas if high chemical stability is necessary. However, these materials have some disadvantages in advanced technology implementations. Namely, it is not possible to use diamond as a cutting tool for ferrous alloys at high temperatures and c-BN is weaken at high temperatures and transforms to the layered hexagonal structure (h-BN). Tremendous investigations have been performed to fabricate new superhard materials for the industrial applications [3–7].

The ultra-hard or hard materials having the commercial importance are mostly composed of light elements and hence boron rich (B-rich) compounds are good candidates [2] because they have short interatomic bond lengths and strong covalent bonds [8,9]. These characteristics of these compounds yield outstanding chemical (high chemical inertness), physical (low mass density, high thermal conductivity etc.) and mechanical (high hardness, excellent wear resistance etc.) features [8,10,11]. In summary, B-rich compounds with these characters have a remarkable importance for the nuclear industry [12], thermoelectric applications [13,14], catalysis [15] and hydrogen storage [16,17] and thus, they are considered as strategic materials.

Among B-rich compounds, boron suboxides (B_xO, $x>1$) have a great attention in the industrial areas due to their promising and outstanding properties such as high hardness, low density, high tensile strength, semiconductivity, high chemical stability and large bulk moduli. B_2O phase has a special place as an "unsymmetrical" analogue of carbon [18–21]. Even though the high temperature/pressure syntheses of B_2O in both graphite-like [18,20] and diamond-like [20] was discussed, the later studies propounded that these phases of B_2O were not stable [22,23]. Apart from B_2O structure, B_xO phases having different stoichiometry ($x = 4$, 6, 7, 8, 10, 12, 16, 18, 20, 22 and 26) were also synthesized and analyzed [19,24,25]. Amongst these structures, B_6O has gotten a special attention and is the most extensively investigated one because it is accepted as the hardest material (indeed the hardest oxide) after diamond and c-BN. B_6O crystallizes in two structures, namely, α-B_6O [26] and β-B_6O [27,28]. α-B_6O has an α-boron (α-B) crystal structure that can be represented by an oxygen-stuffed phase of α-B [27]. α-B_6O can be described as a cubic close packing (ccp, ABCABC… stacking) of the icosahedral B_{12} unit with two oxygen atoms occupying all octahedral spaces in it [27]. Besides, the crystal structure of α-B_6O is closely associated with that of boron carbide (c-BC) [9]. α-B_6O, as in c-BC, has a

* Corresponding author.
E-mail address: murat.durandurdu@agu.edu.tr (M. Durandurdu).

https://doi.org/10.1016/j.jnoncrysol.2022.122130
Received 17 October 2022; Received in revised form 3 December 2022; Accepted 29 December 2022
Available online 20 January 2023

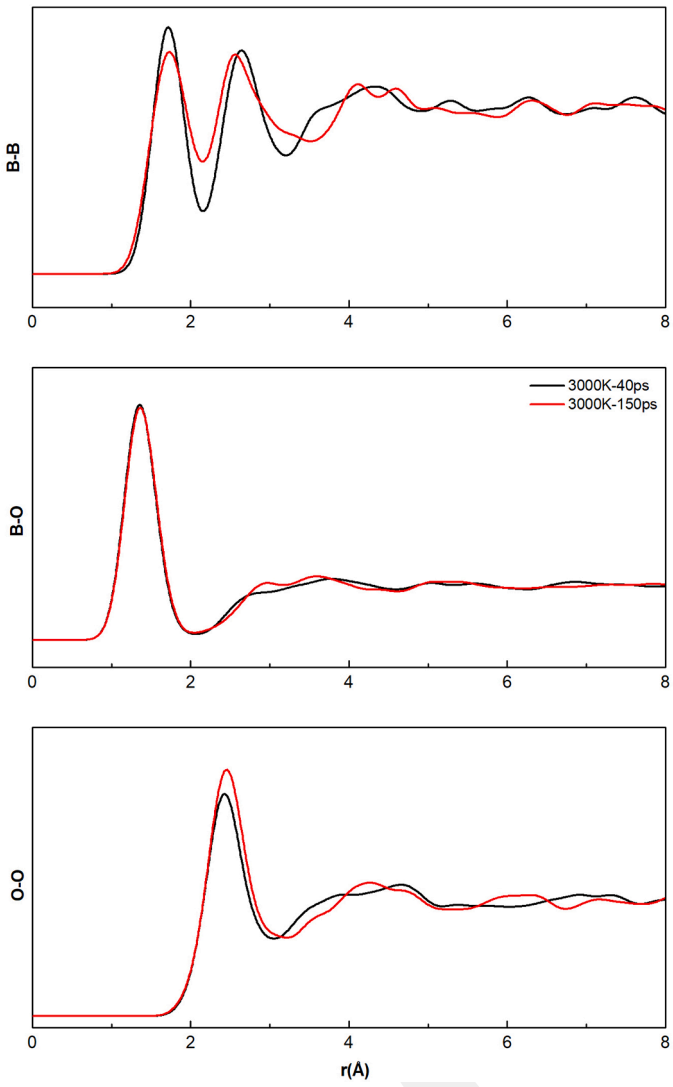

Fig. 1. The PPDFs of the $B_{50}O_{50}$ system thermalized for 40 ps and 150 ps at 3000 K.

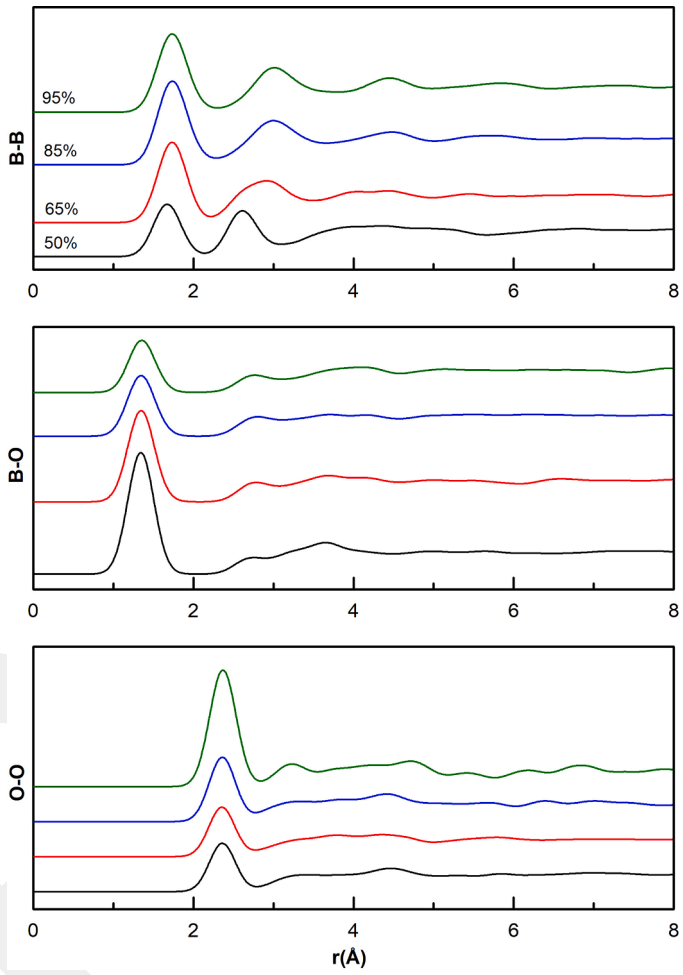

Fig. 2. The PPDFs of a-B_xO_{1-x} at some B concentrations.

wide composition range resulting from the non-complete filling at the oxygen atom positions between the icosahedral B_{12} units. On the other hand, β-B_6O, a new phase of B_6O, was asserted by both theoretical and experimental studies [27,28]. β-B_6O, similar to α-B_6O, is derived from *β*-B phase with an oxygen-stuffed in it and is based on a hexagonal close packing (hcp, ABAB… stacking) [27]. It was shown that most properties (volume, hardness, elastic moduli and DFT band gaps) of α- and β-B_6O structures are very similar each other [27].

In addition to the crystalline forms, amorphous boron suboxides (a-B_xO) can be fabricated by using different experimental protocols, for example, a hot pressing, a reactive radio frequency (RF) magnetron sputtering, an evaporation and a cathodic arc deposition [1,29-34]. Additionally, *ab initio* molecular dynamics (AIMD) [35–37] and classical molecular dynamics (MD) [32] simulations were executed to shed lights on some properties of a-B_xO compounds. The main focus on these experimental and theoretical studies was the mechanical (specifically hardness) and electrical properties of a-B_xO. Apart from these investigations, a high-pressure study reported that the B_6O structure transformed from the crystal phase to an amorphous phase comprising of glassy boron (a-B) and amorphous boron trioxide (a-B_2O_3) upon pressure release [38]. Furthermore, the shear-induced amorphization was observed in B_6O during the nanoindentation process [39]. Later, the amorphization of B_6O was theoretically scrutinized by using an *ab initio* dynamics simulation [40].

Most experimental and theoretical investigations in the literature are related to c-B_6O and there have been limited studies on the amorphous forms. Consequently, their atomic structure and electrical and mechanical properties have not yet been explained in details. The present work is based on AIMD simulations and has two main objectives: the first one is the creation of B-rich amorphous boron oxides (a-B_xO_{1-x}, $0.5 \leq x \leq 95$, some compositions have not been investigated before) and the second one is to shed some lights onto the influence of B concentration on their local structure and mechanical properties.

2. Methodology

All AIMD calculations of B-rich a-B_xO_{1-x} ($0.5 \leq x \leq 0.95$) were carried out via SIESTA code that is based on the density functional theory (DFT) [41] with the generalized gradient approximations (GGA) as parameterized by Lee, Yang and Parr (LYP) for exchange–correlation functions [42,43]. The calculations were performed at the Γ-point of the Brillouin zone (BZ) and double-zeta (DZ) was used as the basis sets. The pseudopotential for B- and O-atoms was generated by using the Troullier

Table 1
The shortest distances r_{ij} (*i,j* are types of atoms) between atoms for all amorphous models.

r_{ij}	r_{BB}	r_{BO}	r_{OO}	Theoretical/Experimental	References
Phase					
Amorphous					
$B_{50}O_{50}$	1.67	1.34	2.36	Theoretical	This study
$B_{55}O_{45}$	1.72	1.35	2.36	Theoretical	This study
$B_{60}O_{40}$	1.73	1.35	2.37	Theoretical	This study
$B_{65}O_{35}$	1.73	1.34	2.35	Theoretical	This study
$B_{70}O_{30}$	1.74	1.35	2.36	Theoretical	This study
$B_{75}O_{25}$	1.73	1.34	2.36	Theoretical	This study
$B_{80}O_{20}$	1.72	1.35	2.36	Theoretical	This study
$B_{85}O_{15}$	1.73	1.34	2.36	Theoretical	This study
$B_{90}O_{10}$	1.76	1.37	2.38	Theoretical	This study
$B_{95}O_{5}$	1.73	1.35	2.36	Theoretical	This study
B	1.78			Theoretical	[52]
	1.80			Experimental	[53]
	1.75	1.37		Theoretical	[36]
B_6O					
Crystal	1.68	1.37	2.41	Theoretical	This study
B_2O					
	1.75	1.58	2.57	Theoretical	[47]
	1.75–1.86	1.35–1.39		Theoretical	[48]
B_2O_3	2.54	1.34	2.37	Theoretical	This study
	2.75	1.35	2.60	Theoretical	[54]
		1.37–1.46		Theoretical	[55]
B_6O	1.76	1.50	3.31	Theoretical	This study
	1.70–0.1.81	1.50	3.01	Theoretical	[49]
		1.46–0.1.48	3.00–3.03	Experimental	[50]
	1.68–1.83	1.43–1.46	3.05–3.08	Experimental	[51]

and Martins scheme [44]. AIMD simulations were executed within the isothermal–isobaric ensemble. The velocity scaling and the Parrinello-Rahman methodologies [45] were preferred to control temperature and pressure, respectively. Each AIMD time step was selected to be 1.0 fs. The starting configuration was a BN melt having almost no chemical disorder and a mean coordination number of about 3.0. In the first step, a-$B_{50}O_{50}$ structure was constructed from the BN melt by replacing N atoms with O atoms (100 B atoms and 100 O atoms). In order to create other B-rich B_xO_{1-x} phases ($0.55 \leq x \leq 0.95$), B atoms were randomly substituted with O atoms until the structure reached to the projected B concentration. Thuswise, ten different networks were generated to be simulated. Then, the supercells were exposed to an initial temperature which was determined roughly from BO phase diagram [22] and it was in the range of 3000 K (50 at.% B)−2500 K (95 at. % B). In our earlier work on B_6O [36], the simulation time of 40 ps was found to be enough to have an equilibrated melt. Nonetheless in the present study, the $B_{50}O_{50}$ system was thermalized for 150 ps at different temperatures of 2500–3000 K and the structure at 40 ps and 150 ps was compared. The partial pair distribution functions (PPDFs) shown in Fig. 1 reveal no significant topological difference between these two structures. For the structure at 40 ps, the mean coordination number of B and O atoms was found to be 3.06 and 1.96, respectively and for the structure at 150 ps, the average coordination number of B and O atoms was determined to be 3.07 and 1.95, correspondingly. Since there is no significant difference in the first coordination shell of the structure at 40 ps and 150 ps, the other compositions were equilibrated for only 40 ps at their initial temperature. These configurations were then quenched to the room temperature (300 K) in ~200–250 ps. The final structures at 300 K were relaxed by using a conjugate gradient (CG) approximation until the maximum force on atoms is smaller than 0.01 eV/Å. All amorphous networks were visualized by means of VESTA software [46]. Lastly, the crystalline B_2O, B_2O_3 and B_6O structures were studied for compression purposes.

3. Results

3.1. Local Structure

In order to assess the primary structural description of each amorphous model, PPDFs are elucidated as a first step of our analysis and some examples are plotted in Fig. 2. The B-B, B-O and O—O correlations for all B contents exhibit a clear well-defined first peak, which is the main character of an amorphous structure. To understand the effect of B concentration on the average bond lengths of the simulated materials, the peak position of the first B-B and B-O coordination shells (r_{ij}) are perceived and presented in Table 1 along with the available data in the literature. The mean B-B bond length increases with increasing B content and it is in the range of 1.67–1.76 Å. The range predicted is well-comparable with the previous experimental and theoretical results of 1.68–1.86 [47–51] (Table 1). Additionally, for high B content materials, the average B-B bond separation is in a good accordance with 1.78 and 1.80 Å in a-B [52,53]. On the other hand, the mean B-O bond length is projected to be between 1.34–1.37 Å. Subsequently, one can see that B concentration has practically no impact on this bond separation. This is due to the fact that the coordination number of O atoms remains almost the same for all compositions (see below). The B-O bond length (1.34–1.37 Å) predicted is parallel to 1.34–1.35 Å in c-B_2O_3 [54,55] but it is considerably shorter than 1.43–1.50 Å in c-B_6O [36,49-51]. This shortening conceivably denotes the polymerization of the B-O units and the formation of B_3O_2 type local structures in the simulated amorphous configurations. Lastly, the O—O bonding does not form in any models.

In the next step, we acquire another important parameter, the mean coordination number, to offer an additional description of the local structure of the amorphous networks. The average coordination number of B- and O-atoms are determined by using the first minimum of the related PPDFs (i.e., cut-off radii, 2.14–2.30 Å for the B-B pair and 2.01–2.09 Å for the B-O pair depending upon the B content) and their variation as a function of B concentration is depicted in Fig. 3. The

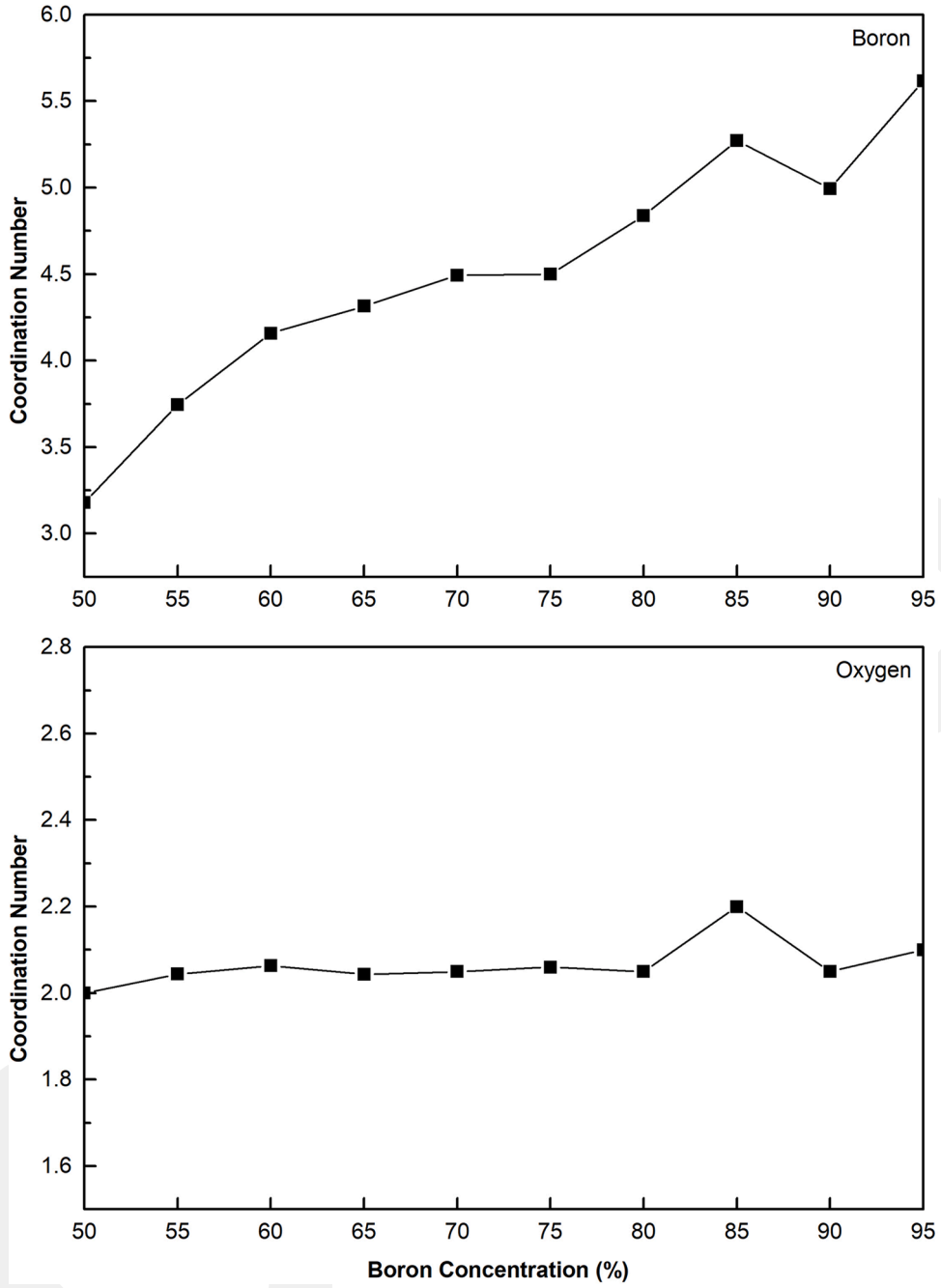

Fig. 3. The modifications in average coordination number of B- and O-atoms as a function of B content.

average coordination of B atom radically changes from 3.18 to 5.62 with increasing B/O ratio. The mean coordination of B atom at low B contents is comparable with 3.0 in c-B_2O and c-B_2O_3 while between 70 and 95 at. % B, it is close to 6 as in c-B_6O, c-B and a-B [56]. Perhaps the most extraordinary observation is unaffected O-coordination; it is about 2.0 for all compositions. Among the BO materials, O-atoms in B_2O_3 (glass or crystal) are twofold coordinated while they are threefold coordinated in c-B_6O. This finding provides an additional support for B-O polymerization in all amorphous network.

In order to have particular knowledge regarding the atomic structure of the models, we investigate their coordination distribution and our results are illustrated in Fig. 4. As B concentration rises, the fraction of threefold coordinated B atoms importantly declines from 81% to ~5% whilst that of sixfold coordinated B atoms alters from 3% to ~55% (see in Fig. 4). The frequency of fourfold and fivefold coordinated motifs of B atoms increases with increasing B content as well. Lastly, a trivial amount of sevenfold coordinated B atoms develops in some amorphous models. As for O atoms, the models have a large fraction of twofold and a small fraction of threefold coordinated motifs.

The Voronoi polyhedron analysis [57,58] can shed some lights on the sorts of clusters formed around B atom. A Voronoi polyhedron can be constructed by connecting perpendicular bisectors between a central

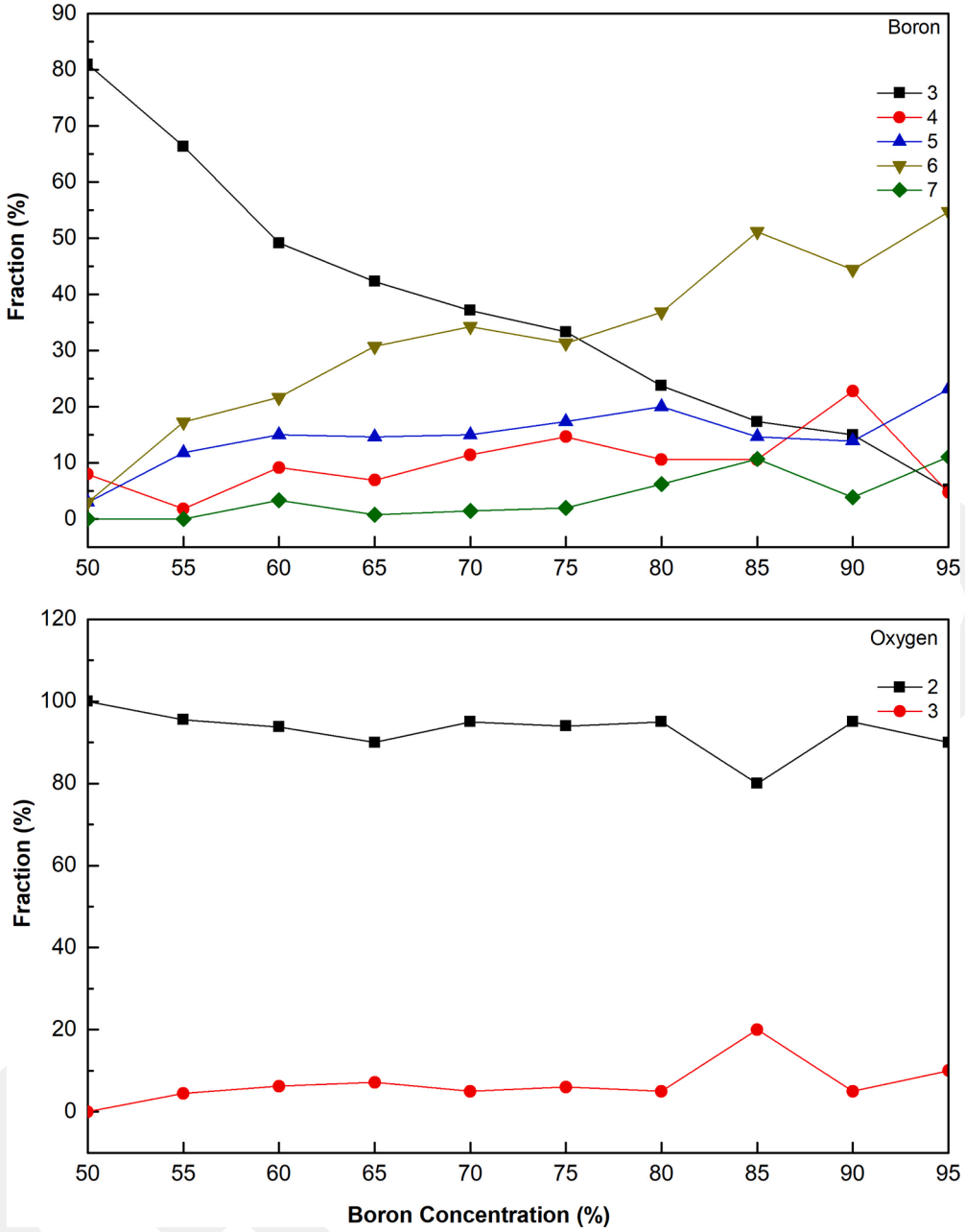

Fig. 4. The coordination distributions of B and O atoms as a function of B concentrations.

atom and all of its neighboring atoms and is identified by the topological Voronoi index (n_3, n_4, n_5,…), where n_i is the number of i-edge faces of a polyhedron around certain atom and $\Sigma\, n_i$ represents the total coordination number of the corresponding polyhedron. We focus on certain polyhedra having high frequencies, especially, produced by B_{12} icosahedra. The B_{12} icosahedron that is a key unit of most B/B-rich materials in both the crystalline and amorphous forms consists of the pentagonal-pyramid structure (B_6). In the Voronoi analysis, the pentagonal-pyramid-like structures can form in the way of complete or incomplete (or defective). The complete pentagonal-pyramid-like clusters are represented by ⟨2, 2, 2, 0⟩ type index while the incomplete or defective ones are described by ⟨2, 3, 0, 0⟩ index. The fraction of these indices for B atoms is shown in Fig. 5. Note that even a-$B_{50}O_{50}$ has a small amount of these clusters and with increasing B content their fraction drastically increases, implying that B atoms have a strong tendency to form B_{12} molecules.

All computer-generated configurations were visualized and the ball-stick representation of some models is presented in Fig. 6. One can see the occurrence of chemical segregations and the formation of possible B-rich and O-rich regions (B:B_2O_3 phase separations). Indeed, in a high pressure experiment on B_6O, the formation of a-B_6O was recovered upon pressure release and the recovered sample consists of a-B_2O_3 and a-B domains, parallel to our observation [38].

We further calculate the bond angle distributions (BADs) for each amorphous network and some of them are plotted in Fig. 7. When the B-B-B angles are considered, as for 50% and 55% B contents, they show a broad distribution changing from about 88° to 140° but a sharp peak at about 60° appears in the distribution. In addition to this angle, another sharp peak at ~107° develops at 60% and higher B concentrations. These two angles are indeed originated from the bonds of the pentagonal pyramids like motifs. By considering the B-O-B angles, all BADs demonstrate a broad distribution in the range of ~108°-170° but have a noticeable one around 135°, parallel to that of c-B_2O_3. The O-B-O angles in the simulated models possess a main peak at around 120°, similar to

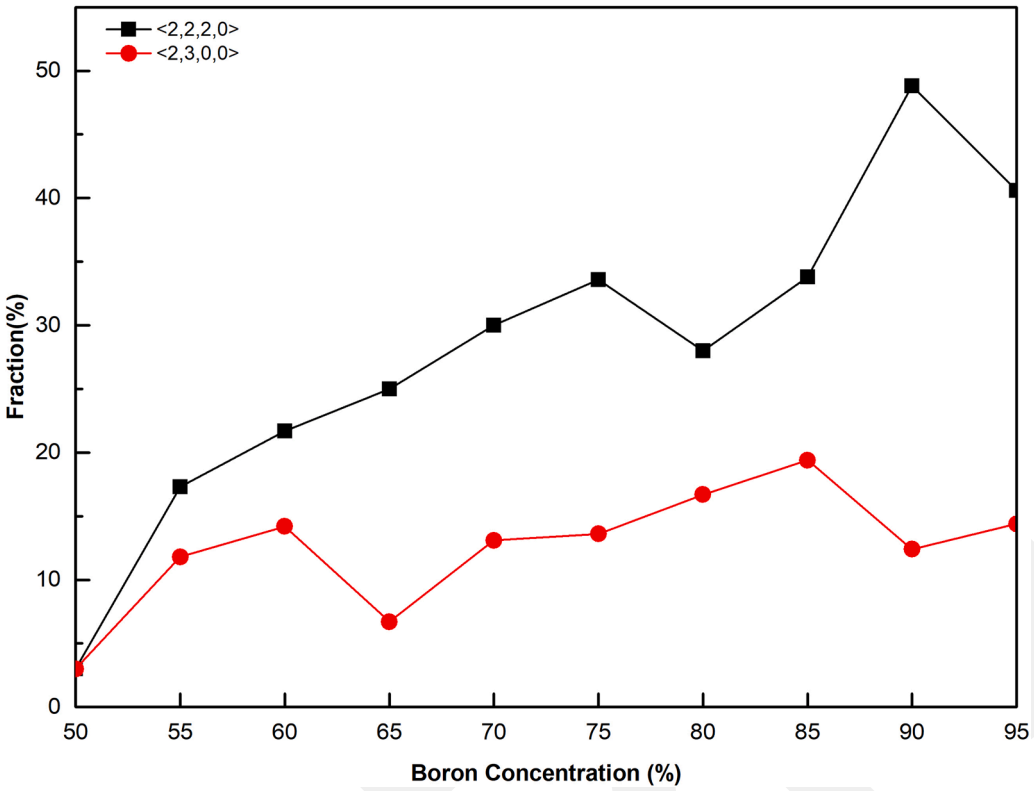

Fig. 5. The fractions of ⟨2, 2, 2, 0⟩, ⟨2, 3, 0, 0⟩ and ⟨4, 0, 0, 0⟩ type indices as a function of B content.

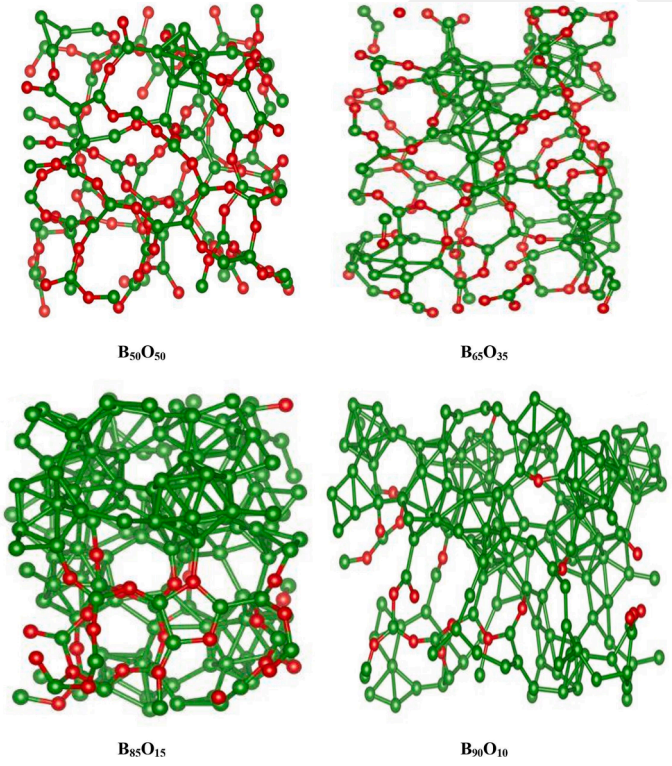

Fig. 6. The ball-stick representations of the simulated amorphous networks.

those of B_2O and B_2O_3 crystals.

3.2. Mechanical Properties

The applications of an engineering material in technology requires the knowledge about its mechanical characteristics. For this reason, we consider the mechanical features of each amorphous configuration in details. We first probe the bulk modulus (K) that can be readily calculated by fitting the energy (E)-volume (V) correlation to the third-order Birch-Murnaghan equation of states,

$$E(V)=E_o+\frac{9V_OK}{16}\left\{\left[\left(\frac{V_o}{V}\right)^{\frac{2}{3}}-1\right]^3K'+\left[\left(\frac{V_o}{V}\right)^{\frac{2}{3}}-1\right]^2\left[6-4\left(\frac{V_o}{V}\right)^{\frac{2}{3}}\right]\right\} \quad \text{(I)}$$

where $K' = dK/dP$ (P is pressure) and the subscript "0″ means the equilibrium values. The alteration of K as a function of B content is illustrated in Fig. 8 and given in Table 2 as well. For comparison purpose, the accessible data in the literature are also provided in the same table. The K value of the amorphous materials drastically changes from ~21 GPa to ~182 GPa. This increasing trend in bulk modulus is thought to be originated from the development of more B_{12} molecules at high B contents. At low B contents, the K values predicted are comparable with the experimental or theoretical values of ~10–18 GPa in a-B_2O_3 [59] and c-B_2O_3 [22] and 24 GPa in c-B_2O [47]. Our estimations beyond 80% B concentrations are approximately overlapped with the previous experimental and theoretical findings of 106 GPa for a-B_6O [36] and 109–272 GPa for a-BO_x (x: 0.02– 0.28) [31]. Moreover, the K value at 95% B content is ~182.4 GPa, comparable with 213 GPa (experimental) [60] and 193 GPa (theoretical) in c-B [61].

Poisson's ratio of a material subjected to a uniaxial stress can be

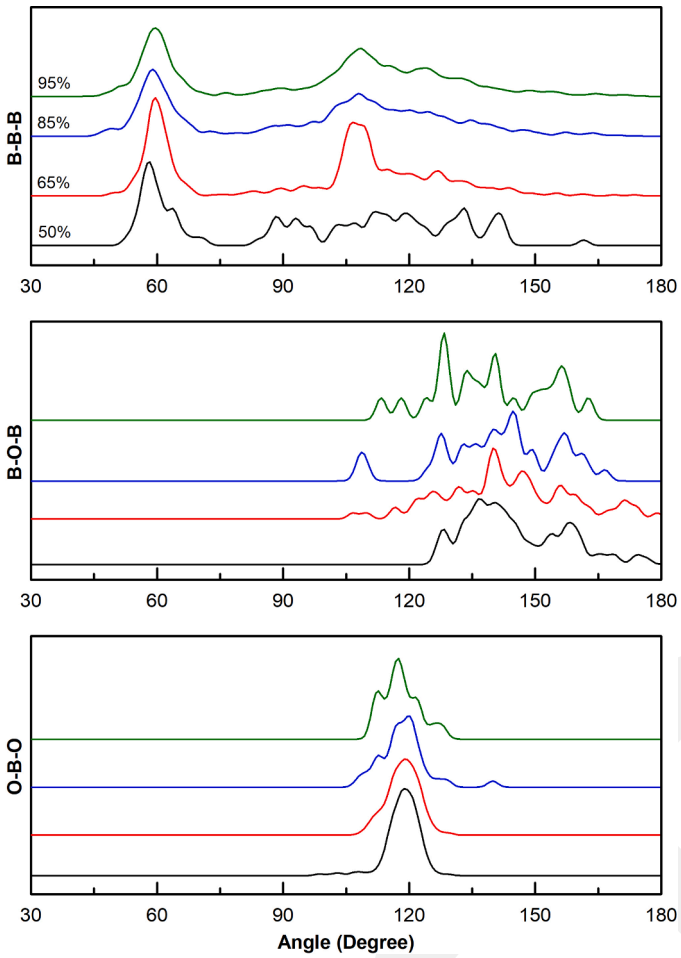

Fig. 7. BADs in some B contents.

expressed as

$$\nu ij = -\frac{\Delta L_i / L_i}{\Delta L_j / \Delta L_j} \quad \text{(II)}$$

here i and j denote the transfer and applied strain directions, correspondingly and Ls are the magnitude of the diagonal terms of the supercell's vectors. We apply a uniaxial stress along the principal axis of each model and observe the changes along transfer directions to estimate Poisson's ratio. In this way, we perceive six different values for Poisson's ratio from the best linear fitting. The average value of ν is given in Fig. 8. ν shows a decreasing trend and changes from ~0.35–0.21 that are in coherent with the values of 0.15, 0.18 and 0.2 for c-B_6O [49], a-B_6O [36] and a-BO_x (x: 0.02– 0.28) [31], respectively. It should be noted here that because of the fitting, some errors in Poisson's ratio projected are expected.

Young's modulus (E) is calculated using the following equation;

$$E = 3K(1 - 2\nu). \quad \text{(III)}$$

It tends to increase overall from 23 to 312 GPa (see Fig. 9 and Table 2), indicating that the materials become less elastic with increasing B concentration. Our estimated value for a-$B_{85}O_{15}$ (~200 GPa) is parallel to the theoretical result of ~203 GPa in a-B_6O [36].

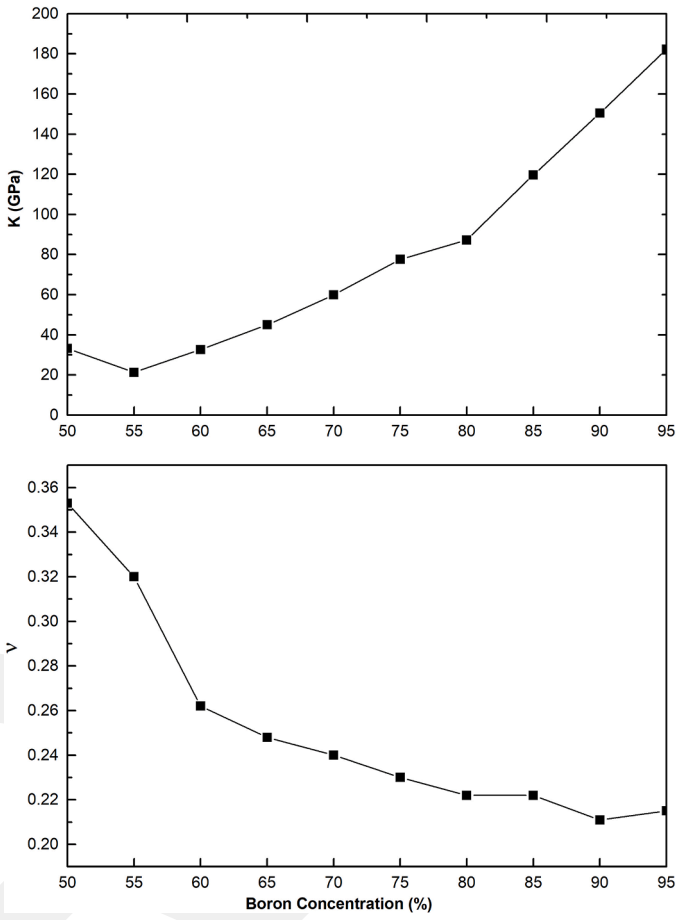

Fig. 8. Variation in bulk modulus (K) and Poisson ratio (ν) as a function of B concentration.

However, the reported experimental and theoretical E values for c-B_6O (470–540 GPa) [11,49,62,63] and c-B (470 GPa) [1] (Table 2) are very much higher than our findings.

Since we acquire E and ν values, shear modulus (μ) can be easily computed as

$$\mu = \frac{E}{2(1+\nu)}. \quad \text{(IV)}$$

Shear modulus of the simulated amorphous models increases from ~9 GPa to ~128 GPa (see Fig. 9) with increasing B content. The calculated value of a-$B_{85}O_{15}$ (~82 GPa) is again analogue to that of a-B_6O (~86 GPa) [36] computed in the earlier theoretical work. Yet, the estimated μ values for c-B_6O (206–227 GPa) structure in the previous works [11,27,55,62,64,65] are also noticeably greater than ours (Table 2). The smaller result in the amorphous forms signifies that they have more a flexible structure than the crystalline forms.

In addition to these mechanical parameters, we evaluate the Vicker's hardness (H_v) using the next four empirical equations [66–69]

$$H_v = 0.151\mu \quad \text{(V)}$$

$$Hv = 2\left(\frac{\mu}{n^2}\right)^{0.585} - -3(\text{GPa}) \quad \text{(VI)}$$

Table 2
Bulk (K), young (E) and shear (μ) moduli, poisson ratios (ν) and Pugh's ratio (n). K, E, μ and H_v are in the unit of GPa.

	K	*ν*	E	μ	*n*	H_v	References
Phase							
Amorphous							
$B_{50}O_{50}$	33.2	0.35	29.2	10.8	3.068	−0.83–1.86	*This study*
$B_{55}O_{45}$	21.3	0.32	23.0	8.7	2.444	−0.51–1.54	*This study*
$B_{60}O_{40}$	32.6	0.26	46.6	18.5	1.768	2.66–3.79	*This study*
$B_{65}O_{35}$	25.3	0.25	38.3	15.3	1.651	4.12–5.40	*This study*
$B_{70}O_{30}$	59.9	0.26	85.2	33.7	1.776	5.70–7.09	*This study*
$B_{75}O_{25}$	77.6	0.26	112.2	44.6	1.741	7.72–9.27	*This study*
$B_{80}O_{20}$	87.3	0.22	145.6	59.6	1.465	8.99–10.97	*This study*
$B_{85}O_{15}$	119.7	0.22	199.6	81.7	1.465	12.33–13.81	*This study*
$B_{90}O_{10}$	150.4	0.21	260.9	107.7	1.397	16.27–17.90	*This study*
$B_{95}O_5$	182.4	0.22	311.9	128.4	1.421	19.19–19.81	*This study*
B_6O	106	0.18	203	86		13–18	[36]
B_2O_3	10						[59]
BO_x*	109–272	0.2					[31]
Crystal							
B_2O	24	0.68					[47]
B_2O_3	10–18						[22]
						1.5 ± 5	[70]
B_6O	181–300		470–540	206–227			[11,27,62,64 65]
	209.4–246	0.15	480–507.8	208–223.1		38–38.2	[27,49]
						33–36	[2]
						45	[8]
B_xO**						32–60	[71]
Boron	213		470			35	[60]
	193						[61]

*BO_x thin films; *x*: 0.02– 0.28,.
**B_xO; *x*:2, 4, 6, 7, 8, 10, 12, 18, 20, 22.
Ref. [27,36,47,49,61,64,65] are theoretical works,.
Ref. [1,2,8,11,20,31,60,62,63] are experimental works.

$$Hv = 0.92\left(\frac{1}{n}\right)^{1.137}(\mu)0.708 \quad \text{(VII)}$$

and

$$Hv = 0.0635\text{E} \quad \text{(VIII)}$$

where $n = K/\mu$ is referred as the Pugh's ratio. The results obtained from these equations are exposed in Fig. 10. The hardness shows an increasing trend and is in the range of 1.3 to 19.8 GPa. Our predictions for the certain B content are comparable with the experimental result of 1.5 ± 5 GPa for c-B_2O_3 structure [70], but some are noticeably less than the experimental data of 32–60 GPa in c-B_xO (*x*:2, 4, 6, 7, 8, 10, 12, 18, 20, 22), c-B_6O and c-B [2,8,27,60,61,71]. We should note here that the negative values obtained for some compositions is due to the limitation of equation VI (see Ref. [68] for more information).

In addition to the Vicker's hardness, the microhardness value (H) of each model is also calculated by using next equation [72]

$$H = \frac{(1-2\nu)\text{E}}{6\,(1+\nu)}(\text{GPa}) \quad \text{(IX)}$$

and illustrated in Fig. 11. The H value of the models changes from 1.05 GPa to 24.4 GPa depending on B concentration. We find no data in the literature to compare our estimations.

Lastly, the determining of brittle-ductile characteristic of any material has a big importance in the advanced technological applications. This characteristic can be specified by two different ways, Poisson's ratio and Pugh's ratio (*n*) [73,74]. (Fig. 12) 1.75 is believed as the critical value for *n*. If *n* is smaller (bigger) than the critical value, the material presents the brittle (ductile) feature. On the other hand, if the Poisson's ratio is less (higher) than 0.26, the material exhibits brittle (ductile) character. For some amorphous materials, the values of *n* and *ν* (Table 2) are in the range of 1.768–3.068 and 0.26–0.35, correspondingly. Consequently, it can be expressed that the B-rich amorphous materials up to 70–75% concentration show a ductile character while the others exhibit a brittle feature.

4. Discussion

An extensive investigation on B-rich a-B_xO_{1-x} ($0.5 \leq x \leq 0.95$) materials is carried out to expose their features. Our simulations reveal two important structural features in these materials. The first one is that the coordination number of O atoms is almost independent on the composition while that of B atoms steadily increases from 3.18 to 5.62. The local structure around O atoms is found to be fairly parallel to that of B_2O_3 consisting of twofold coordinated O-atoms. The second one is the occurrence of chemical segregation in the disordered networks, which becomes obvious for above 60% B content and results in possible B:B_2O_3 phase separations. The occurrence of phase separations involves a long-range diffusion of B and O atoms. Such a diffusion happens in the liquid state of all compositions (noted that the liquid state of some or all compositions might be a hypothetical liquid state at zero pressure because B_6O decomposes at ambient pressure [75] but it can be melted under pressure [76,77]) in even short-simulation times. Indeed, phase separations occur in the liquid states and are preserved during the fast solidification procedure. We should note here that the development of the crystalline B and B_2O_3 phases was observed during the fast quenched liquid state of B_6O at a pressure of 5.8 GPa whereas a slow quenching rate leads to the crystallization to B_6O, specifying a high-energy barrier for the development of the B_6O crystal [77]. Consequently, it might be

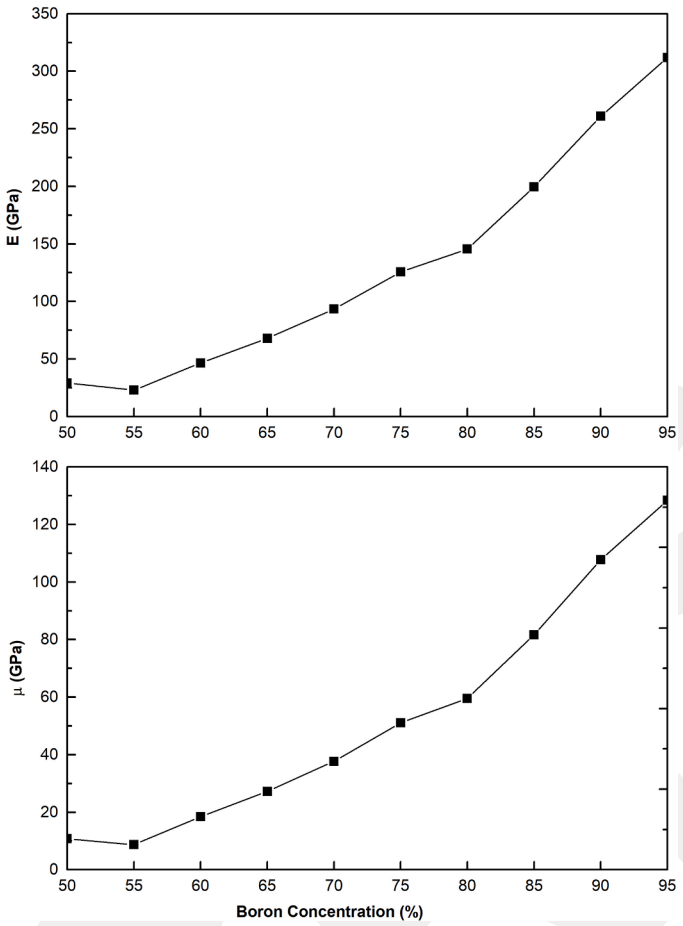

Fig. 9. Variation in young (E) and shear (μ) modulus vs B content.

unsurprising to see the amorphous B and B_2O_3 phases rather than the crystalline ones in the simulations considering the very fast quenching rate used in the simulation, relative to experiment. Using the same simulation technique, the relative energy difference is between the amorphous and the crystalline phases of B_6O is estimated to be 0.35 eV/atom [36], suggesting a fairly surmountable energy barrier between these phases. These experimental findings can be interpreted as the presence of possible phase separations in the liquid phase of B_6O at high pressure(s) as well, supporting our results. Furthermore, a pressure-induced amorphization was observed in c-B_6O on decompression and resulting a-B_6O consists of a-B_2O_3 and a-B domains, which also validate our findings. Yet unlike a-B_2O_3, boroxol rings are not observed in our models. The formation of such rings has not been discussed in the earlier work on a-B_xO [29–37] as well. It is known that the formation of the rings requires a long simulation time. We simulate $B_{50}O_{50}$ more than 150 ps at different temperatures as mention in the method section but we do not observe a drastic structural change between the configuration at 40 ps and 150 ps and detect the formation boroxol rings in the structure. Here we can speculate some possibilities for no existing rings in the models: i) It might possible that the compositions studied do not allow to the development of such rings, ii) it is also likely that even 150 ps is not enough for the development of boroxol rings for the compositions simulated and iii) it is possible that the size of the simulation box is not large enough, namely the size of B_2O_3 domains are not large enough for the development of the rings. Probably a machine-learning potential on a larger system for a long simulation time can clarify this issue.

As B concentration increases, the coordination number of B atom increases because B atoms have a strong tendency to form pentagonal pyramid-like structures and hence B_{12} icosahedrons. Their formation has a dramatic influence on the mechanical properties. Namely they increase with increasing B content, in agreement with the previous investigation on a-B_xO. Yet when the mechanical properties of amorphous network are compared with the crystalline counterpart, a radical decrease in the mechanical properties is detected in the amorphous forms. This is probably due to the formation of soft B_2O_3-like regions in the models.

Within the limitation of DFT and approximations used to estimate the mechanical properties of the amorphous models, our simulation also reveals a region where there is a ductile-to brittle transition in the amorphous materials, which corresponds to 70–75% B concentrations. We should note here that Pugh's ratio approach was proposed for polycrystalline materials while Poisson ratio approach was proposed for metallic glasses and hence there might be some uncertainties for composition at which the transition occurs.

5. Conclusions

Boron oxides are commonly studied materials. These materials,

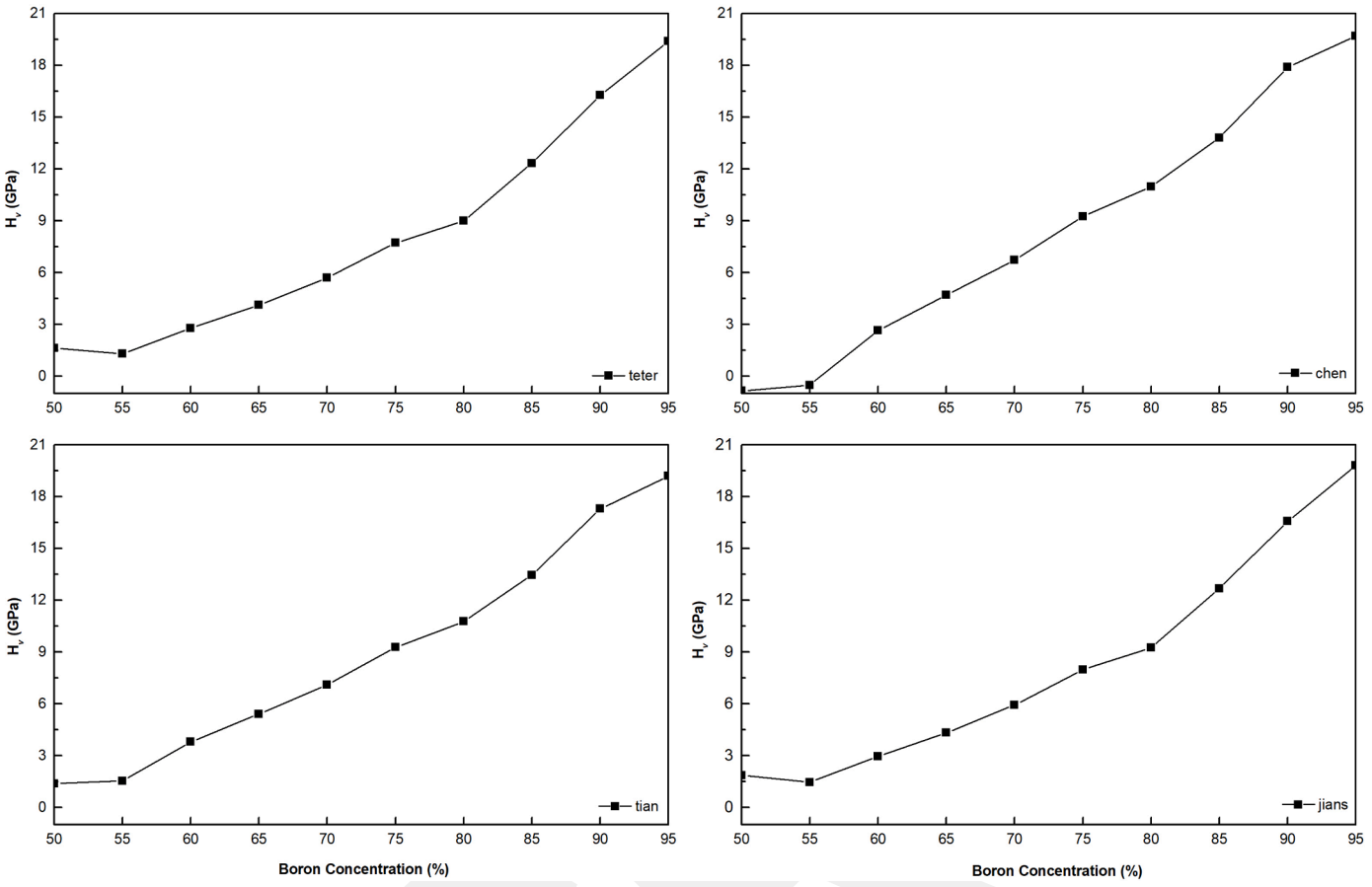

Fig. 10. B concentration dependence of Vickers hardness (H).

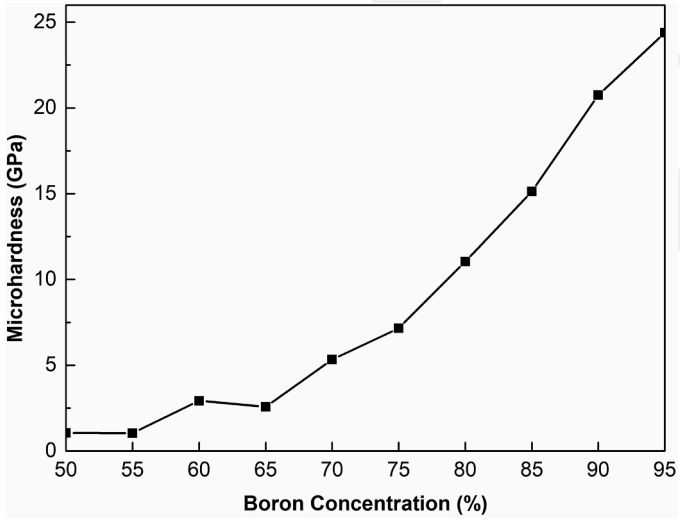

Fig. 11. B concentration dependence of the alterations in microhardness (H_v).

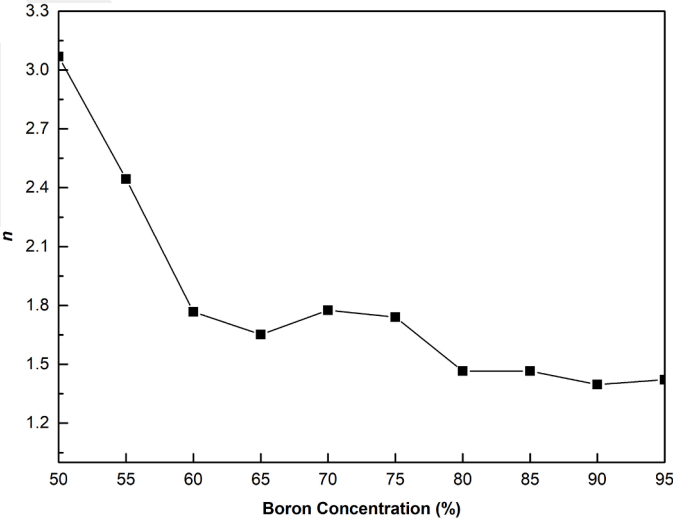

Fig. 12. Variation in Pugh's ratio (n) vs B content.

especially boron suboxide, have a world-wide attention due to their high bulk modulus and high indentation hardness. For this reason, we have generated amorphous B_xO_{1-x}, ($0.5 \leq x \leq 95$) configurations by means of AIMD simulations and their microstructure and mechanical features have been scrutinized. The mean B-coordination increases from 3.18 to 5.62 but the mean O-coordination remains almost null and about 2.0 as in B_2O_3. B:B_2O_3 phase separations are observed in most materials modelled. The bulk modulus of the models is found to be between ~21–182 GPa. The Vicker's hardness is estimated to be in the range of −0.51–19.81 GPa. The amorphous materials (B_xO_{1-x}, $x \geq 80$) are classified as hard materials. Within the limitations of DFT and approaches used, we speculate that there is a ductile-to-brittle transition at around 70–75% B contents.

CRediT authorship contribution statement

Ayşegül Özlem Çetin Karacaoğlan: Investigation, Validation, Formal analysis, Data curation, Writing – original draft, Visualization. **Murat Durandurdu:** Conceptualization, Methodology, Resources, Supervision, Funding acquisition, Writing – review & editing.

Declaration of Competing Interest

The authors declare that they have no known competing financial interests or personal relationships that could have appeared to influence the work reported in this paper.

Data availability

Data will be made available on request.

Acknowledgements

The authors are thankful to the Scientific and Technological Research Council of Turkey (TÜBİTAK) under MAG award 117M372. AÖK acknowledges partial financial support from YÖK 100/2000 and TÜBİTAK BİDEB 2211-C programs. We acknowledge computing time provided by the TÜBİTAK High Performance and Grid Computing Center (TRUBA resources).

References

[1] S.M. Gorbatkin, R.L. Rhoades, T.Y. Tsui, W.C. Oliver, Hard boron oxide thin-film deposition using electron cyclotron resonance microwave plasmas, Appl. Phys. Lett. 65 (21) (1994) 2672–2674.
[2] M. Herrmann, I. Sigalas, M. Thiele, M.M. Müller, H.J. Kleebe, A. Michaelis, Boron suboxide ultrahard materials, Int. J. Refract. Hard Met. 39 (2013) 53–60.
[3] M. Olofsson, T. Lundström, Synthesis and structure of non-stoichiometric B6O, J. Alloys Compd. 257 (1–2) (1997) 91–95.
[4] H. Hubert, L.A. Garvie, B. Devouard, P.R. Buseck, W.T. Petuskey, P.F. McMillan, High-pressure, high-temperature synthesis and characterization of boron suboxide (B6O), Chem. Mater. 10 (6) (1998) 1530–1537.
[5] I. Solodkyi, S.S. Xie, T. Zhao, H. Borodianska, Y. Sakka, O. Vasylkiv, Synthesis of B6O powder and spark plasma sintering of B6O and B6O–B4C ceramics, J. Ceram. Soc. Jpn. 121 (1419) (2013) 950–955.
[6] S.S. Xie, H. Chen, I. Solodkyi, O. Vasylkiv, A.I. Tok, Cyclic formation of boron suboxide crystallites into star-shaped nanoplates, Scr. Mater. 99 (2015) 69–72.
[7] I. Solodkyi, H. Borodianska, T. Zhao, Y. Sakka, P. Badica, O. Vasylkiv, B6O ceramic by in-situ reactive spark plasma sintering of a B2O3 and B powder mixture, J. Ceram. Soc. Jpn. 122 (1425) (2014) 336–340.
[8] D. He, Y. Zhao, L. Daemen, J. Qian, T.D. Shen, T.W. Zerda, Boron suboxide: as hard as cubic boron nitride, Appl. Phys. Lett. 81 (4) (2002) 643–645.
[9] B. Albert, H. Hillebrecht, Boron: elementary challenge for experimenters and theoreticians, Angew. Chem. Int. Ed. 48 (46) (2009) 8640–8668.
[10] A. Zerr, R. Riedel, Introduction: novel ultrahard materials, Handb. Ceram. Hard Mater. 1 (2000) 45–73.
[11] T.C. Shabalala, D.S. McLachlan, I. Sigalas, M. Herrmann, Hard and tough boron suboxide based composites, Ceram. Int. 34 (7) (2008) 1713–1717.
[12] J. Dai, Z. Tian, Large thermal conductivity of boron suboxides despite complex structures, Appl. Phys. Lett. 118 (4) (2021), 041901.
[13] H. Wang, Q. An, Band-gap engineering in high-temperature boron-rich icosahedral compounds, J. Phys. Chem. C 123 (19) (2019) 12505–12513.
[14] T. Mori, T. Nishimura, K. Yamaura, E. Takayama-Muromachi, High temperature thermoelectric properties of a homologous series of n-type boron icosahedra compounds: a possible counterpart to p-type boron carbide, J. Appl. Phys. 101 (9) (2007), 093714-093714.
[15] Y. Chen, et al., Highly active, nonprecious electrocatalyst comprising borophene subunits for the hydrogen evolution reaction, J. Am. Chem. Soc. 139 (36) (2017) 12370–12373.
[16] Z. Huang, S. Wang, R.D. Dewhurst, N.V. Ignat'ev, M. Finze, H. Braunschweig, Boron: its role in energy-related processes and applications, Angew. Chem. Int. Ed 59 (23) (2020) 8800–8816.
[17] S. Satyapal, J. Petrovic, C. Read, G. Thomas, G. Ordaz, The US Department of Energy's National Hydrogen Storage Project: progress towards meeting hydrogen-powered vehicle requirements, Catal. Today 120 (3–4) (2007) 246–256.
[18] H.T. Hall, L.A. Compton, Group IV analogs and high pressure, high temperature synthesis of B2O, Inorg. Chem. 4. 8 (1965) 1213–1216.
[19] X.Y. Liu, X.D. Zhao, W.H. Su, High pressure synthesis of serial higher boron suboxides with cage structures, in: AIP Conference Proceedings 309, American Institute of Physics, 1994, pp. 1279–1282.
[20] T. Endo, T. Sato, M. Shimada, High-pressure synthesis of B 2 O with diamond-like structure, J. Mater. Sci. Lett 6 (6) (1987) 683–685.
[21] A.V. Nemukhin, F. Weinhold, Boron oxides: ab initio studies with natural bond orbital analysis, J. Chem. Phys. 98 (2) (1993) 1329–1335.
[22] V.L. Solozhenko, O.O. Kurakevych, V.Z. Turkevich, D.V. Turkevich, Phase diagram of the B–B2O3 system at 5 GPa: experimental and theoretical studies, J. Phys. Chem. B 112 (21) (2008) 6683–6687.
[23] M.P. Grumbach, O.F. Sankey, P.F. McMillan, Properties of B2O: an unsymmetrical analog of carbon, Phys. Rev. B 52 (22) (1995) 15807–15811.
[24] V. Srikanth, R. Roy, E.K. Graham, D.E. Voigt, BxO: phases present at high pressure and temperature, J. Am. Ceram. Soc. 74. 12 (1991) 3145–3147.
[25] X. Liu, X. Zhao, W. Hou, W. Su, A new route for the synthesis of boron suboxide B7O, J. Alloys Compd. 223 (1) (1995) L7–L9.
[26] H. Hubert, B. Devouard, L.A. Garvie, M. O'Keeffe, P.R. Buseck, W.T. Petuskey, P. F. McMillan, Icosahedral packing of B12 icosahedra in boron suboxide (B6O), Nature 391 (6665) (1998) 376–378.
[27] H. Dong, et al., Prediction of a new ground state of superhard compound B6O at ambient conditions, Sci. Rep. 6. 1 (2016) 1–6.
[28] Q. An, K.M. Reddy, H. Dong, M.W. Chen, A.R. Oganov, W.A. Goddard III, Nanotwinned boron suboxide (B6O): new ground state of B6O, Nano Lett. 16 (7) (2016) 4236–4242.
[29] C. Doughty, S.M. Gorbatkin, T.Y. Tsui, G.M. Pharr, D.L. Medlin, Hard boron–suboxide-based films deposited in a sputter-sourced, high-density plasma deposition system, J. Vac. Sci. Technol. A 15 (5) (1997) 2623–2626.
[30] C.C. Klepper, et al., Amorphous boron coatings produced with vacuum arc deposition technology, J. Vac. Sci. Technol. A: 20 (3) (2002) 725–732.
[31] D. Music, et al., Synthesis and mechanical properties of boron suboxide thin films, J. Vac. Sci. Technol. A 20 (2) (2002) 335–337.
[32] D. Music, U. Kreissig, V. Chirita, J.M. Schneider, U. Helmersson, Elastic modulus of amorphous boron suboxide thin films studied by theoretical and experimental methods, J. Appl. Phys. 93 (2) (2003) 940–944.
[33] D. Music, et al., Role of carbon in boron suboxide thin films, J. Vac. Sci. Technol. A 21 (4) (2003) 1355–1358.
[34] D. Music, U. Kreissig, Z.S. Czigány, U. Helmersson, J.M. Schneider, Elastic modulus-density relationship for amorphous boron suboxide thin films, Appl. Phys. A 76 (2) (2003) 269–271.
[35] D. Music, J.M. Schneider, Elastic properties of amorphous boron suboxide based solids studied using ab initio molecular dynamics, J. Phys. Condens. Matter 20 (19) (2008), 195203-195203.
[36] M. Durandurdu, Amorphous boron suboxide, J. Am. Ceram. Soc. 102 (8) (2019) 4546–4554.
[37] M. Durandurdu, High pressure modifications in amorphous boron suboxide: an ab initio study, Ceram. Int. 46 (5) (2020) 5968–5975.
[38] Z. Wang, Y. Zhao, P. Lazor, H. Annersten, S.K. Saxena, In situ pressure Raman spectroscopy and mechanical stability of superhard boron suboxide, Appl. Phys. Lett. 86 (4) (2005), 041911.
[39] K.M. Reddy, A. Hirata, P. Liu, T. Fujita, T. Goto, M.W. Chen, Shear amorphization of boron suboxide, Scr. Mater. 76 (2014) 9–12.
[40] C. Kunka, Q. An, N. Rudawski, G. Subhash, J. Zheng, V. Halls, J. Singh, Nanotwinning and amorphization of boron suboxide, Acta Mater 147 (2018) 195–202.
[41] P. Ordejón, E. Artacho, J.M. Soler, Self-consistent order-N density-functional calculations for very large systems, Phys. Rev. B 53 (16) (1996) R10441–R10444.
[42] A.D. Becke, Density-functional exchange-energy approximation with correct asymptotic behavior, Phys. Rev. A 38 (6) (1988) 3098.
[43] C. Lee, W. Yang, R.G. Parr, Development of the Colle-Salvetti correlation-energy formula into a functional of the electron density, Phys. Rev. B 37 (2) (1988) 785.
[44] N. N. Troullier, J.L. Martins, Efficient pseudopotentials for plane-wave calculations Phys. Rev. B 43 (3) (1991) 1993–2006.
[45] M. Parrinello, A. Rahman, Polymorphic transitions in single crystals: a new molecular dynamics method, J. Appl. Phys. 52 (12) (1981) 7182–7190.
[46] K. Momma, F. Izumi, VESTA 3 for three-dimensional visualization of crystal, volumetric and morphology data, J. Appl. Crystallogr. 44 (6) (2011) 1272–1276.
[47] https://materialsproject.org/materials/mp-614006/#.
[48] J. Wang, Q. Li, C.J. Pickard, C. Chen, Y. Ma, Computational discovery and characterization of new B2O phases, Phys. Chem. Chem. Phys. 21 (5) (2019) 2499–2506.
[49] A.B. Rahane, V. Kumar, J.S. Dunn, Carbon doping in Boron suboxide: structure, energetics, and elastic properties, J. Am. Ceram. Soc. 98 (7) (2015) 2223–2233.
[50] T. Lundström, Structure and bulk modulus of high-strength boron compounds, J. Solid State Chem. 133 (1) (1997) 88–92.
[51] M. Kobayashi, I. Higashi, C. Brodhag, F. Thevenot, Structure of B6O boron-suboxide by Rietveld refinement, J. Mater. Sci. 28 (8) (1993) 2129–2134.
[52] M. Durandurdu, Liquid boron and amorphous boron: an ab initio molecular dynamics study, J. Non-Cryst. Solids 417 (2015) 10–14.
[53] R.G. Delaplane, U. Dahlborg, W.S. Howells, T. Lundström, A neutron diffraction study of amorphous boron using a pulsed source, J. Non-Cryst. Solids 106 (1–3) (1988) 66–69.
[54] S. Sadaf, T. Wu, L. Zhong, Z.Y. Liao, H.C. Wang, W.L. Wang, Effective mechanism of B2O3 on the structure and viscosity of CaO–SiO2–B2O3-based melts, Steel Res. Int 92 (4) (2021), 2000531-2000531.
[55] H. Dong, et al., Boron oxides under pressure: prediction of the hardest oxides, Phys. Rev. B 98 (17) (2018), 174109-174109.
[56] R. Franz, H. Werheit, Influence of the Jahn-Teller effect on the electronic band structure of boron-rich solids containing B12 icosahedra, in: AIP Conference Proceedings 231, American Institute of Physics, 1991, pp. 29–36.

[57] G. Voronoi, Recherches sur les paralléloèdres primitives, J. Reine Angew. Math 134 (1908) 198–287.
[58] W. Brostow, M. Chybicki, R. Laskowski, J. Rybicki, Voronoi polyhedra and Delaunay simplexes in the structural analysis of molecular-dynamics-simulated materials, Phys. Rev. B 57 (21) (1998) 13448–13458.
[59] V.V. Brazhkin, et al., Nature of the structural transformations in B2O3 glass under high pressure, Phys. Rev. Lett. 101 (3) (2008), 035702-035702.
[60] R.J. Nelmes, J.S. Loveday, D.R. Allan, J.M. Besson, G. Hamel, P. Grima, S. Hull, Neutron-and x-ray-diffraction measurements of the bulk modulus of boron, Phys. Rev. B 47 (13) (1993) 7668–7673.
[61] T. Letsoalo, J.E. Lowther, Systematic trends in boron icosahedral structured materials, Phys. B 403 (17) (2008) 2760–2767.
[62] D.R. Petrak, Mechanical properties of hot-pressed boron suboxide and boron, Ceram. Bull. 53 (1974) 569–573.
[63] B. Goosey, U.S. Patent No. 3,816,586, U.S. Patent and Trademark Office, Washington, DC, 1974.
[64] R.F. Zhang, Z.J. Lin, Y.S. Zhao, S. Veprek, Superhard materials with low elastic moduli: three-dimensional covalent bonding as the origin of superhardness in B6O, Phys. Rev. B 83 (9) (2011), 092101-092101.
[65] Q. An, W.A. Goddard III, Boron suboxide and boron subphosphide crystals: hard ceramics that shear without brittle failure, Chem. Mater. 27 (8) (2015) 2855–2860.
[66] D.M. Teter, Computational alchemy: the search for new superhard materials, MRS Bull. 23 (1) (1998) 22–27.
[67] X.Q. Chen, H. Niu, D. Li, Y. Li, Modeling hardness of polycrystalline materials and bulk metallic glasses, Intermetallics 19 (9) (2011) 1275–1281.
[68] Y. Tian, B. Xu, Z. Zhao, Microscopic theory of hardness and design of novel superhard crystals, Int. J. Refract. Met. Hard. Mater. 33 (2012) 93–106.
[69] X. Jiang, J. Zhao, A. Wu, Y. Bai, X. Jiang, Mechanical and electronic properties of B12-based ternary crystals of orthorhombic phase, J. Phys. Condens. Matter 22 (31) (2010), 315503-315503.
[70] V.A. Mukhanov, O.O. Kurakevych, V.L. Solozhenko, On the Hardness of Boron (III) Oxide, 2011.
[71] Y. Guo, W.A. Goddard, Is carbon nitride harder than diamond? No, but its girth increases when stretched (negative poisson ratio), Chem. Phys. Lett. 237 (1–2) (1995) 72–76.
[72] K. Hussain, et al., Three-dimensional porous borocarbonitride BC2N with negative Poisson's ratio, J. Mater. Chem. C 8 (44) (2020) 15771–15777.
[73] I.N. Frantsevich, Elastic Constants and Elastic Moduli of Metals and Insulators, Reference book, 1982.
[74] S.F. Pugh, XCII. Relations between the elastic moduli and the plastic properties of polycrystalline pure metals, Lond. Edinb. Dublin Philos. Mag. J. Sci. 45 (367) (1954) 823–843.
[75] H.F. Rizzo, W.C. Simmons, H.O. Bielstein, The existence and formation of the solid B_6O, J. Electrochem. Soc. 109 (1962) 1079–1082.
[76] V.L. Solozhenko, C. Lathe, On the melting temperature of B_6O, J. Superhard. Mater. 29 (2007) 259–260.
[77] O.O. Kurakevych, V.L. Solozhenko, Experimental study and critical review of structural, thermodynamic and mechanical properties of superhard refractory boron suboxide B6O, J. Superhard. Mater. 33 (2011) 421–428.